SUPPLEMENTARY INFORMATION

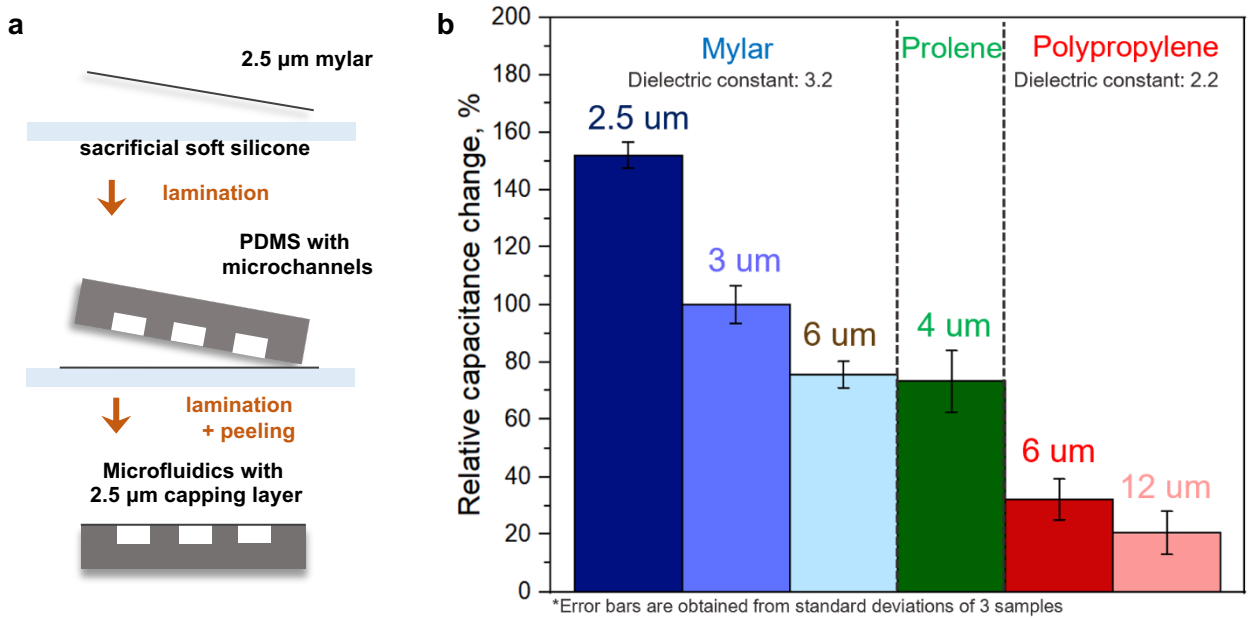

Figure S1: Capping layers for microfluidic channels: Preparation and evaluation of multiple materials and thicknesses

a. **Capping layer preparation for fluidic channels**: a thin sheet (2.5µm Mylar in the example given here, optimal material and thickness chosen for final devices) is laminated on a sacrificial soft silicone as a flat substrate. A piece of PDMS with microchannels laminates onto that substrate. Subsequent peeling provides sealed microchannels capped with the ultra-thin Mylar.

b. **Optimization of capping layer (material and thickness):** a thin film of Mylar, Prolene, or Polypropylene is bonded to a sweat rate microfluidics PDMS channels layer, and the change in capacitance of the interdigitated electrodes laminated on the channels is measured. Ordonnea corresponds to the difference in capacitance between empty channels and channels filled with DI water. Note that adhesion to the interdigitated electrodes is provided in this experiment through a layer of 50:1 base to curing agent ratio Sylgard 184 PDMS, spin coated at 3500 rpm for 5 minutes. Highest sensitivity is achieved with the thinnest Mylar sheet.

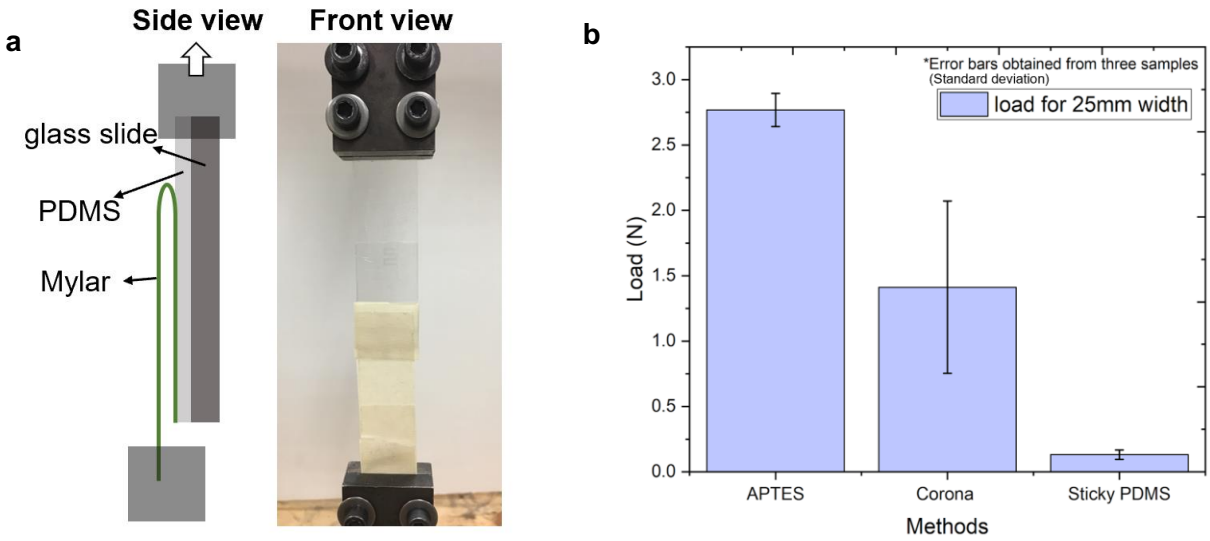

Figure S2: Evaluation of the bonding strength of the capping layer.
The bonding strength between the 2.5 μm Mylar film and the PDMS channel is tested for three bonding methods. Specimens are fabricated by attaching PDMS on a glass slide to prevent detecting the stretch force generated by the PDMS, and the Mylar film is bonded to the PDMS through three different methods: APTES, Corona treatment, and sticky PDMS stamping. APTES treatment includes immersion of the Mylar film in 1:50 APTES solution for 1 h, followed by 30 s of Corona treatment on both Mylar and PDMS pieces, and bonding in the 70^{o}C oven for 24 h. Specimens treated with only Corona treatment is fabricated by treating both Mylar and PDMS specimens for 30 s, followed by thermal bonding (24 h in an oven at 70^{o}C). Steps for sticky PDMS stamping include spin-coating 50:1 sticky PDMS on a glass slide at 3000 rpm for 30 s, laminating PDMS specimen on top of sticky PDMS, peeling off PDMS specimen and laminating it on Mylar film, followed by thermal bonding for 24 h (in an oven at 70^{o}C). Sintech 20G tensile test machine is used to perform a 180^{o} peel test. As shown in frame a, the free end of PDMS is attached on the top grip, while the Mylar is attached with an extended non-elastic mask tape to the bottom grip, all grips and specimen are in the same plane. The machine pulls the Mylar film and the PDMS apart at a rate of 25 mm/min until fully detached. ASTM D903 adhesive peel strength test standard is followed during the test. Constant rectangular cross-section with 25 mm width has remained during the peel test. Graph in figure b shows the bonding strength for the three methods, error bars are obtained from three trials. Among the three bonding methods, Mylar that treated with APTES possesses the highest adhesion to PDMS, with a better reproducibility.

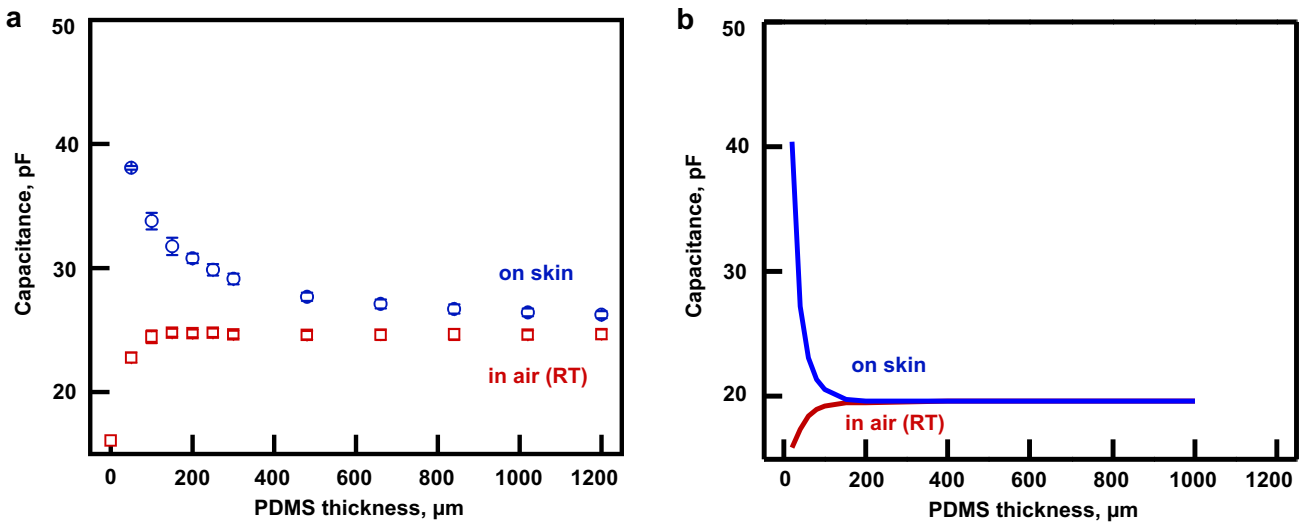

Figure S3: Comparison between experimental and analytical model capacitance values as a function of PDMS thickness on skin and in air at room temperature. The figures above present the dimensional capacitive values, from experiments (a) and analytical model (b), in figure 2b that guide the value of PDMS thickness where the influence of the medium below (air/skin) is minimized. Both experiments and simulation follow the same trend as the capacitance value saturates (i.e. no longer changes for a given PDMS thickness). However, the discrepancy between experiment and analytical model in the absolute value of the saturated capacitance is due to the sensitivity of the dielectric constants for the materials in the sensor.

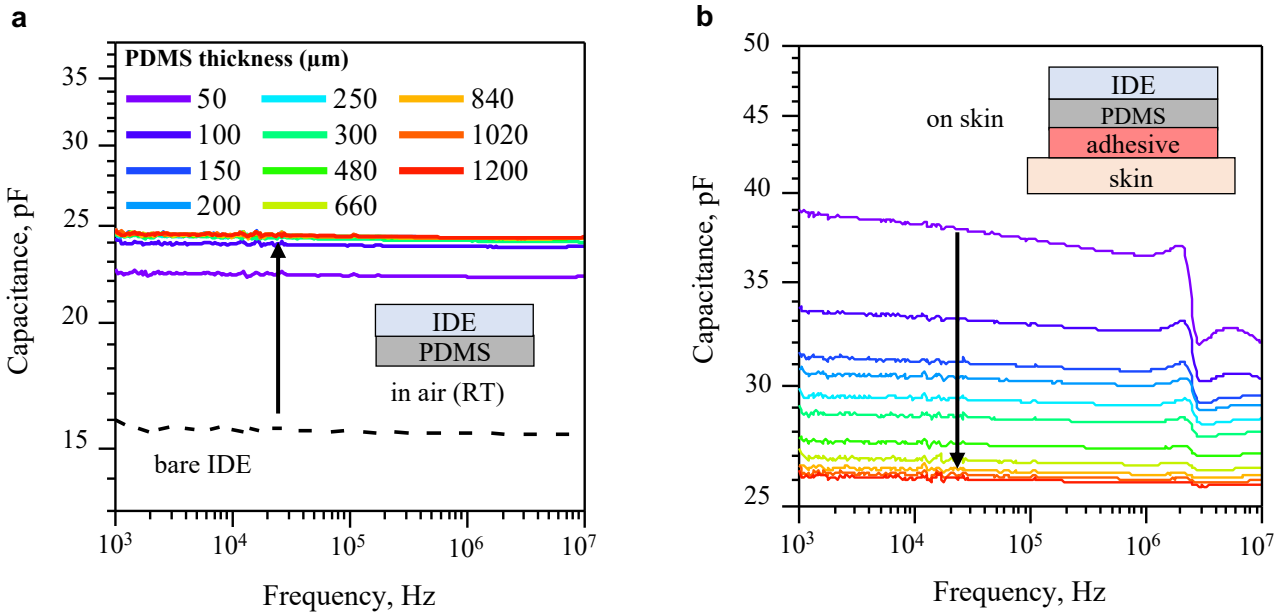

Figure S4: Influence of the presence of a PDMS layer of varying thickness on the capacitance of bare electrodes in air at room temperature (a) and on skin (b).
Typical frequency spectra of capacitance (a) in air and (b) on human skin for a bare IDE (dashed black line) and with 50 to 1200 µm thick layers of PDMS on top of the electrodes (solid colored lines). Corresponding material stacks are shown as figure insets. Arrows indicate capacitance shifts induced by increasing PDMS thickness. Values at 25 kHz from those graphs are extracted and shown in Fig. 2b.

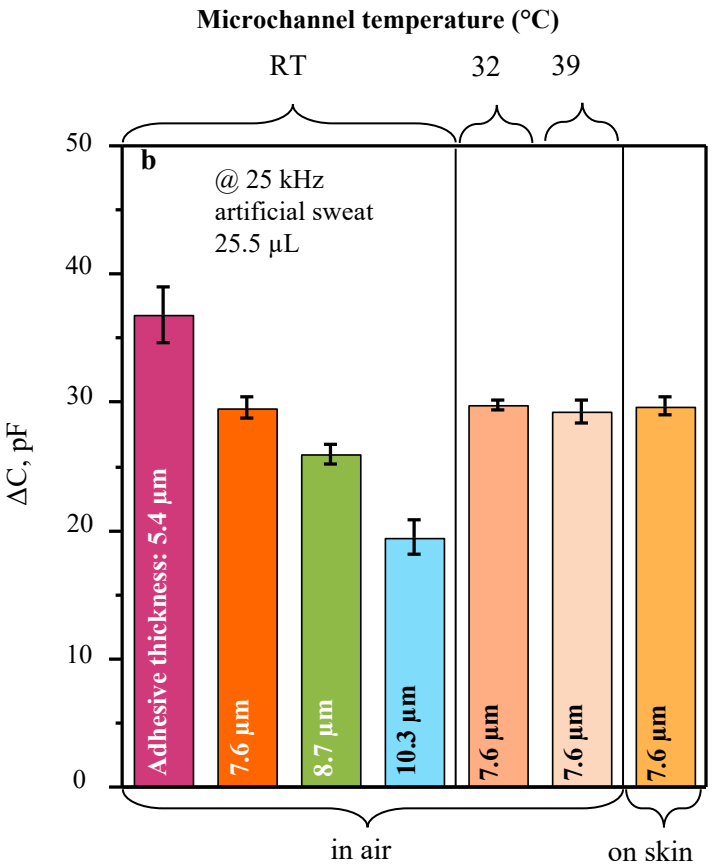

Figure S5: Influence of adhesive thickness, temperature, and skin on the whole range of variation of capacitance between empty and filled channels.
Capacitance change at 25 kHz for completely filled channels for modules with 5.4 (pink), 7.6 (orange), 8.7 (green) or 10.3 µm (blue) thick adhesive at room temperature in air (left box). An optimal adhesive thickness of 7.6 µm is determined with a capacitance change of 29.6 pF enabling a complete utilization of the full-scale range of a promising capacitance read-out chip (FDC1004). The capacitance change for an optimized sensor remains similar when microchannel temperature is increased (middle box) to 32 (light orange) and 39 °C (beige) or when the sensor is applied on human skin (right box, ocher). Error bars were obtained from at least 2 different samples (3 for microchannels with 7.6 µm thick adhesive).

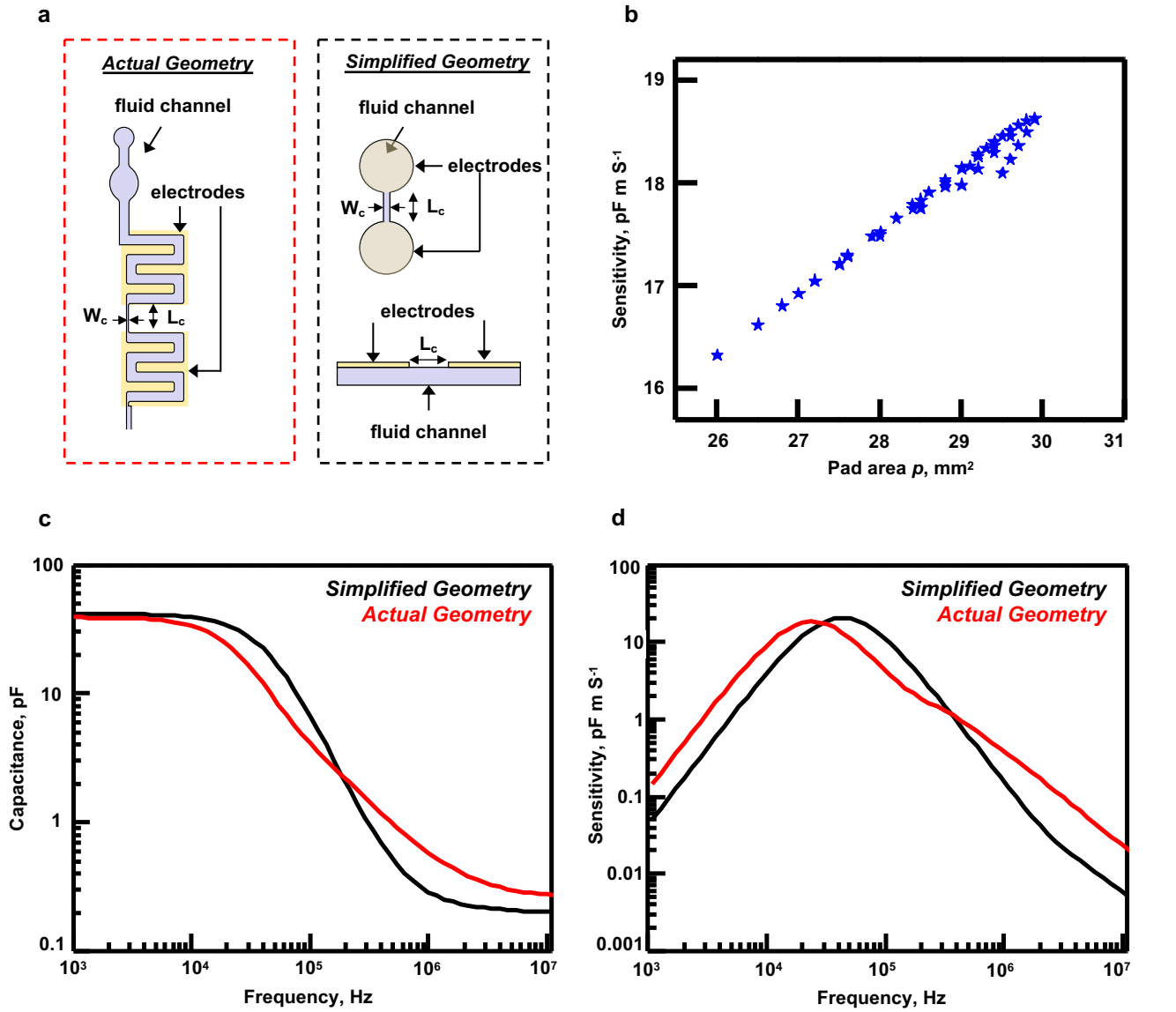

Figure S6: Maximum sensitivity of the sensor as a function of the electrode pad area. The FEA contours for maximum sensitivity and frequency presented in figure 3c and figure 3d assume a constant volume in the parametric study for the connecting channel width $\mathbf{W_c}$ and length $\mathbf{L_c}$. The electrode pad sits directly on top of the circular microfluidic channels to systematically change the area of the circular microfluidic channels and electrode pad when changing $\mathbf{W_c}$ or $\mathbf{L_c}$, while maintaining a constant volume in the microfluidic channels (a). The figure above suggests that increasing the electrode pad area will increase the maximum sensitivity of the sensor (b). It is important to note that for a given connecting channel dimensions, the displayed results are at the frequency where sensitivity is maximum (i.e. figure 3d). Capacitance (c) and sensitivity (d) comparison between the simplified and actual geometry models for a fluid with $\sigma = 1.0 S/m$

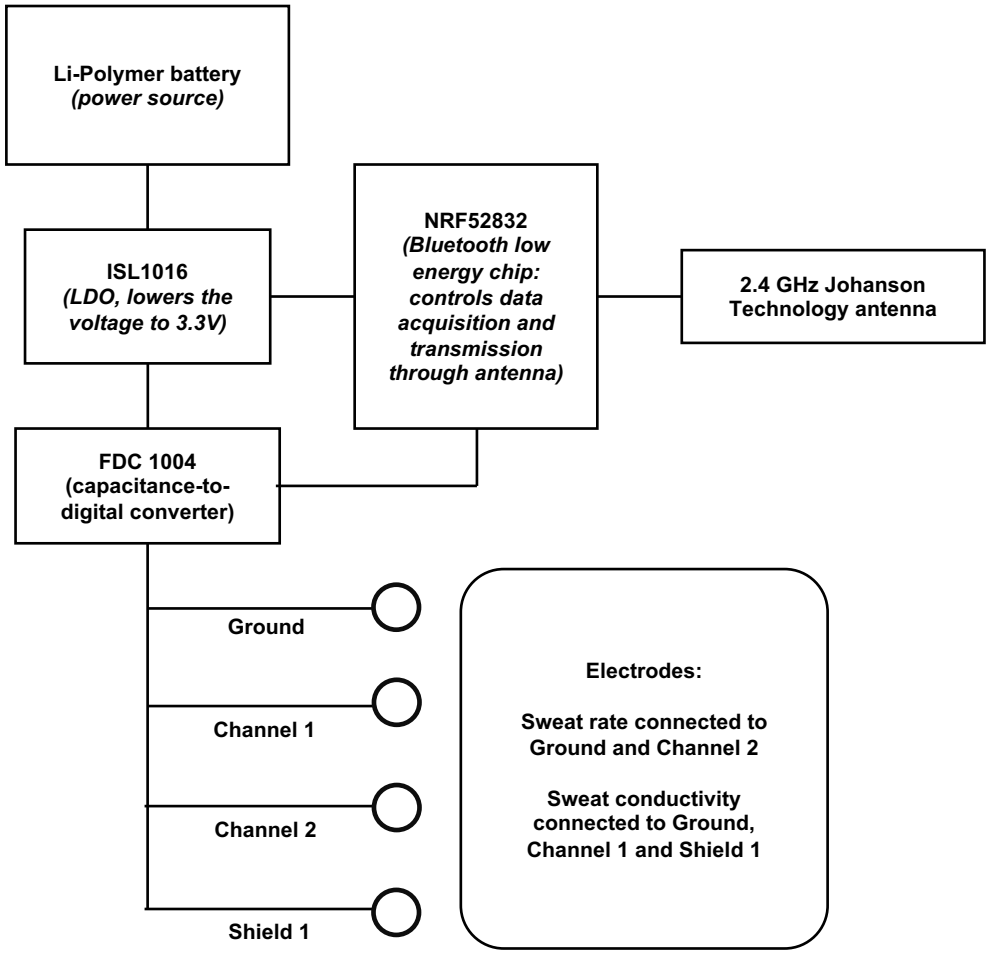

Figure S7: Electronics readout schematics
Schematic presenting the main electronics readout components and the architecture of the electronics layout. Depending on the electrodes (sweat rate or sweat conductivity measurements), two or three of the connection magnets (blue circles) are used to connect the electrodes. In the case of sweat rate channel, measurement is performed between ground and channel 2, and in the case of sweat conductivity channel, measurement is performed between ground and channel 1 with the shielding plane connected to Shield 1.

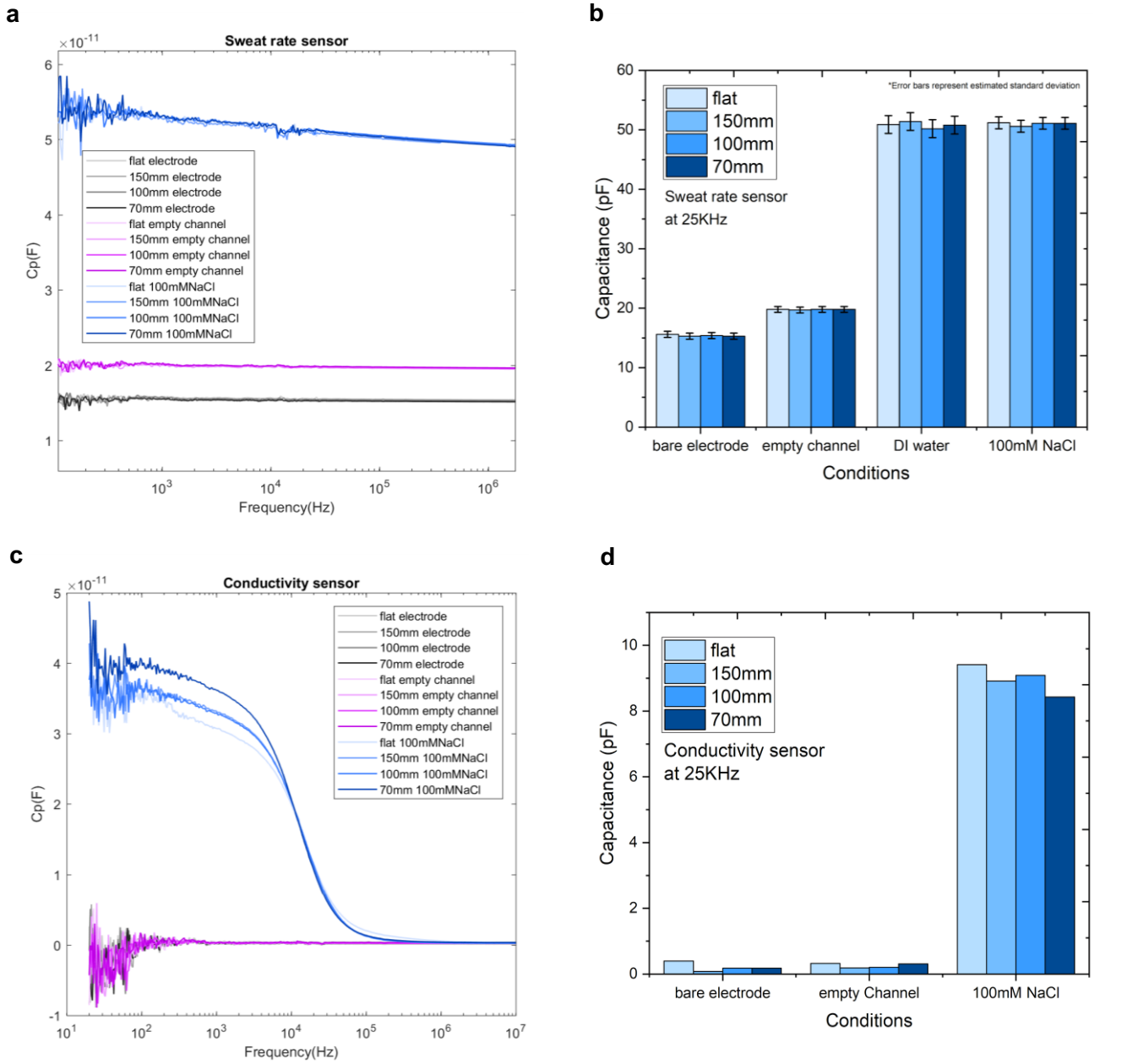

Figure S8: Effects of bending on the results, obtained by attaching the microfluidics channels to PMMA surfaces of various radii of curvature (flat, 150 mm radius 100 mm radius, 70 mm radius). In each case, 3 sets of data are recorded: electrodes only, electrodes on empty microfluidics channels, electrodes on channels filled with 100 mM NaCl (model for sweat). Note that the geometry of conductivity sensor channels and electrodes used for this trial is similar to the final geometry used in main manuscript but not exactly identical.

a. Frequency spectra plot of sweat rate sensor.
b. Capacitance values of sweat rate sensor at 25 kHz under bending.
c. frequency spectra plot of conductivity sensor. Note that geometry of the sensor used in this experiment varies a little from final shape, especially through rounded edges.
d. Capacitance values of conductivity sensor at 25 kHz.

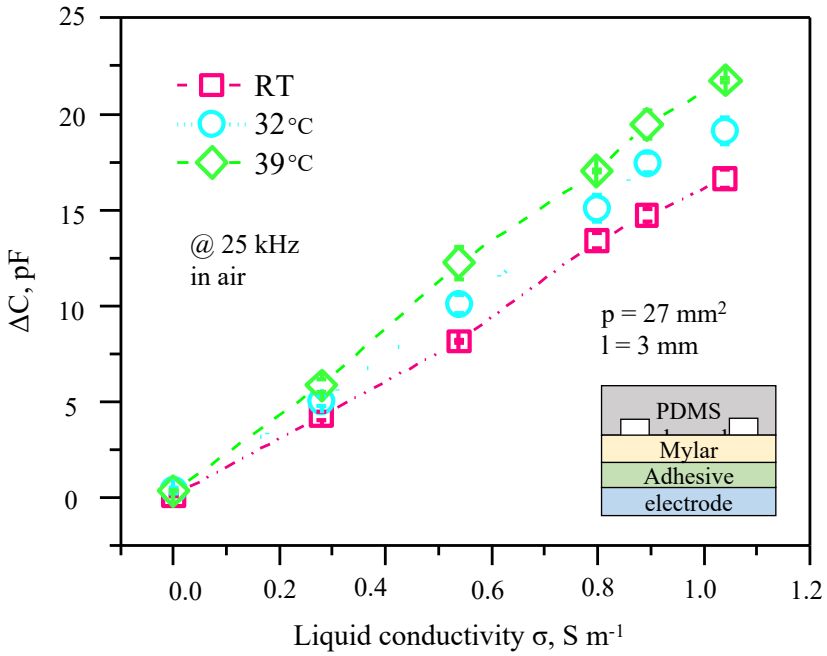

Figure S9: Influence of temperature on the sweat conductivity module:
Capacitance change in air at 25 kHz of an optimized conductivity sensor (p= 27 mm2, l = 3 mm) for liquid conductivities from 0.000179 to 1.04 S m-1 as a function of temperature ranging from room temperature (pink squares, dashed-dotted line) to 32 (turquoise circles, dotted line) and 39 °C (green diamonds, dashed line). With increasing temperature, the capacitance change increases for all investigated conductivities. The material stack of the sensor is shown schematically as an inset.

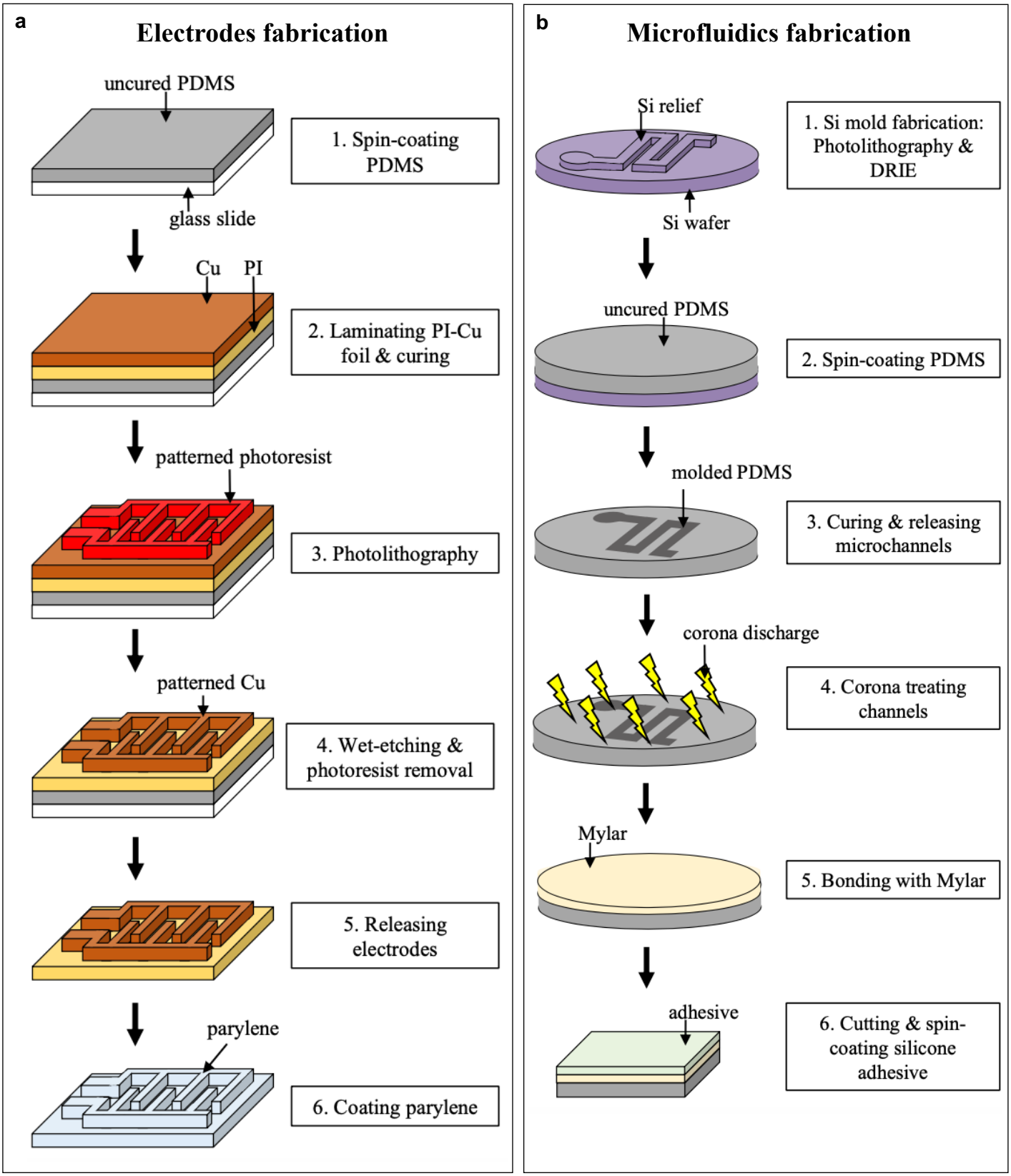

Figure S10: Illustration of the methods used to fabricate the microfluidics and electrodes

a. Schematic illustration of the electrode fabrication process: standard clean-room procedures (photoresist in red) yielded electrode platforms consisting of patterned Cu (brown) on a PI (yellow) supporting layer coated with parylene (light blue). A glass slide (white) coated with PDMS (grey) served as support during fabrication.

b. Fabrication of the microfluidic systems: Photolithography and DRIE produced a Si wafer-based mold (purple). Soft lithography techniques yielded a molded PDMS layer (grey; microchannels in dark grey) that was sealed with Mylar (light yellow) after corona treatment (yellow bolts). Coating of the microfluidic system with silicone adhesive (green) completed the fabrication process.

a

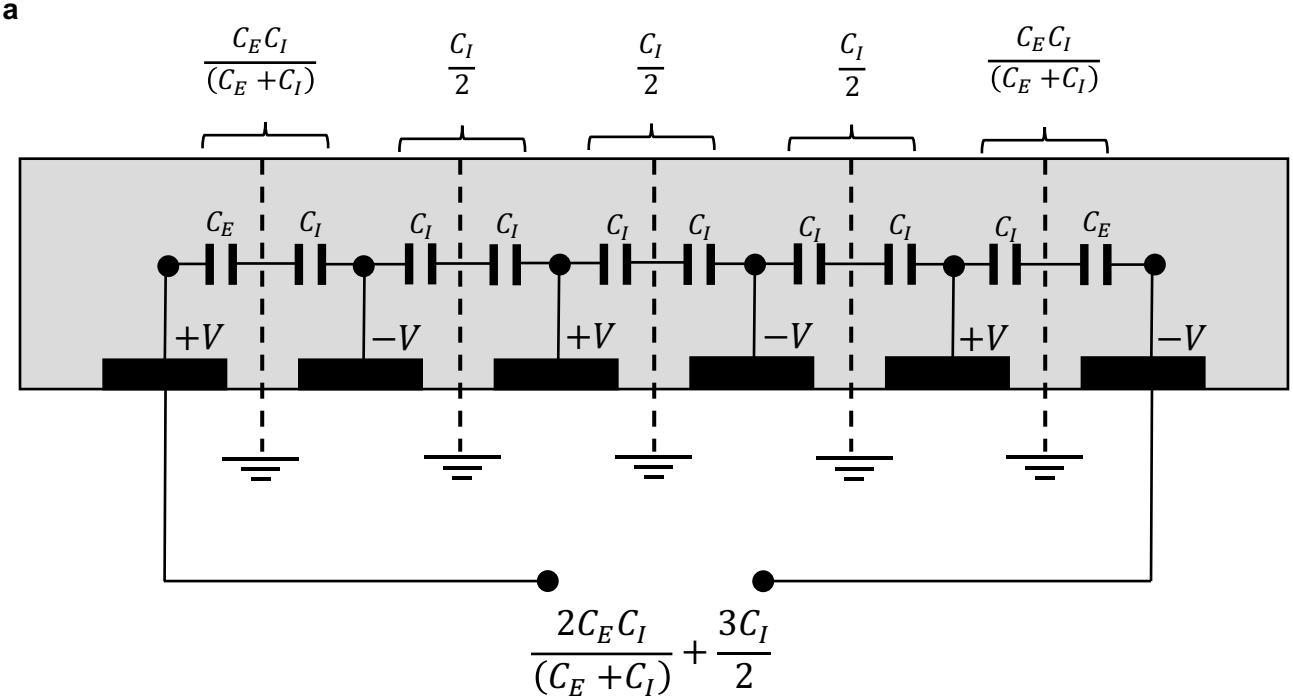

b

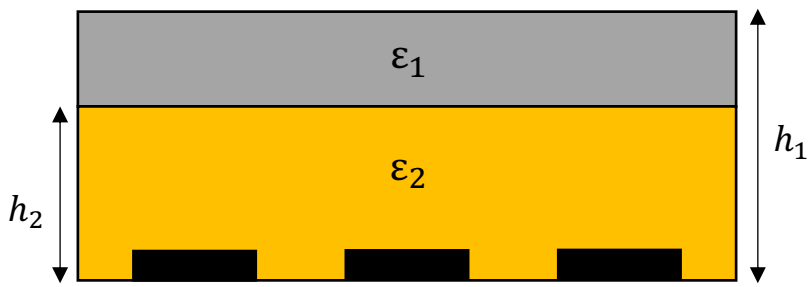

Figure S11: Illustration of the symmetry and layer schematics in the analytical model

a. Example of the equivalent circuit schematic for total capacitance evaluation of a symmetric circuit based on the internal C_I and external C_E capacitance values in the interdigitated electrodes.

b. Partial capacitive contribution from different layers either in parallel ($\varepsilon_1 < \varepsilon_2$) or series ($\varepsilon_1 > \varepsilon_2$) depending on the layer height h and electrode geometry.

Parameter	Air	Dielectric Layer	PDMS	Skin	Fluid
Relative Permittivity ε	1	3.4	2.5	1130.8*	80
Electrical Conductivity σ (S/m)	0	0	0	0	(0-1.04)**
Applied Voltage (V)	1				

*The value of ε is approximated at a frequency of 25 kHz.
**The values of σ vary depending on the conductive solutions in Figure 3a and 3b

Figure S12: Table of parameters used in Analytical/FEM modeling